

Article

# On the Uncertainty of the Image Velocimetry Method Parameters

Evangelos Rozos <sup>\*</sup>, Panayiotis Dimitriadis , Katerina Mazi, Spyridon Lykoudis   
and Antonis Koussis

Institute for Environmental Research & Sustainable Development, National Observatory of Athens,  
GR 152 36 Athens, Greece; pandim@itia.ntua.gr (P.D.); kmazi@noa.gr (K.M.); slykoud@yahoo.com (S.L.);  
akoussis@noa.gr (A.K.)

\* Correspondence: erozos@noa.gr; Tel.: +30-2108-09125

Received: 6 August 2020; Accepted: 3 September 2020; Published: 8 September 2020



**Abstract:** Image velocimetry is a popular remote sensing method mainly because of the very modest cost of the necessary equipment. However, image velocimetry methods employ parameters that require high expertise to select appropriate values in order to obtain accurate surface flow velocity estimations. This introduces considerations regarding the subjectivity introduced in the definition of the parameter values and its impact on the estimated surface velocity. Alternatively, a statistical approach can be employed instead of directly selecting a value for each image velocimetry parameter. First, probability distribution should be defined for each model parameter, and then Monte Carlo simulations should be employed. In this paper, we demonstrate how this statistical approach can be used to simultaneously produce the confidence intervals of the estimated surface velocity, reduce the uncertainty of some parameters (more specifically, the size of the interrogation area), and reduce the subjectivity. Since image velocimetry algorithms are CPU-intensive, an alternative random number generator that allows obtaining the confidence intervals with a limited number of iterations is suggested. The case study indicated that if the statistical approach is applied diligently, one can achieve the previously mentioned threefold objective.

**Keywords:** stream discharge; remote sensing; image velocimetry; LSPIV; Monte Carlo; uncertainty

## 1. Introduction

Streamflow is the fundamental quantity of hydrology and is of paramount importance in studies of surface hydrology [1,2]; however, it is difficult to measure directly. For this reason, the discharge through a cross-section of a stream is estimated in practice indirectly, by converting the readily measured stages  $h$  to flows  $Q$ . It is therefore essential that a stage–discharge relationship  $Q = f(h)$ , a *rating curve*, is established at a stream’s cross-section of interest. This task is accomplished by measuring the velocity field and integrating it over the cross-section of known geometry for a range of flows.

The conventional method of estimating the discharge  $Q$  consists of making a series of water depth and velocity measurements in a number of segments in which the cross-section is divided, and then evaluating the equation ([3], Equation (5.1)):

$$Q \approx \sum a_i v_i, i = 1 \dots n \quad (1)$$

where  $a_i$  is the area of the  $i$ th segment of the measured cross-section,  $v_i$  is the average velocity of the midsection of the  $i$ th segment of the cross-section, and  $n$  is the number of segments (typically, no fewer than 10 and at least 25 for wide rivers [3]). Conventionally, the velocity is sampled manually with

a current meter either at 60% of depth below the free surface (for shallow depths 0.76 m), or at 20% and 80% or at 20%, 60%, and 80% of depth, weighted appropriately to estimate the mean velocity  $v_i$  over the depth ([3] (5.4.5)). It is evident that such campaigns are tedious, costly and at high flows, particularly under flooding conditions, prohibitively dangerous and thus practically impossible.

Advanced alternatives such as the Acoustic Doppler Current Profiler (ADCP) exist, but they are quite expensive. The ADCP measures velocities based on the frequency shift (Doppler effect) of a transmitted signal scattered back to the transceiver from particles in the water ([3] (6.2.2)). It can be installed at fixed locations, e.g., on a riverbank looking sideways, in the bed looking upwards, or mounted on a float, looking downwards, along with acoustic transducers, GPS, and other equipment. The float is towed across the stream performing velocity and bathymetry measurements that yield the velocity field over the depth and along the cross-section [4,5]; its integration gives an estimate of the stream's discharge. However, fixed ADCP installations or applications of floating ADCPs are neither cost-justified nor practical for routine use in small streams, which may additionally be difficult to access. Velocities can also be measured with a portable ADCP by wading in the stream, once again exposing the person making the measurements to the same dangers.

By contrast, estimating the average flow velocity over the depth from the measured surface velocity offers a promising practical means for gauging the discharge of a stream at a cross-section of known bathymetry. The necessary data can be obtained by applying relatively inexpensive remote sensing techniques, either using a hand-held surface flow velocity radar (SVR), or an image velocimetry (e.g., particle image velocimetry, PIV) method [6–10]. In both cases the sensed surface velocity must be translated to the depth-averaged velocity, for example, via multiplication with an empirical coefficient [11], or via hydraulic methods based on the entropy maximization principle that estimate the velocity profile [12–14]. The SVR is a portable equipment of modest cost that directly delivers the surface velocity at selected points along the water surface of a cross-section. The PIV method requires only a camera, preferably equipped with polarization filters to limit glare [15–17], in order to video-scope the stream's surface, but even the ubiquitous smartphone camera may suffice if a discount on data quality is tolerable; however, the PIV data, i.e., the image frames from the video, must be processed to yield velocities. It is worth noting that PIV is becoming increasingly popular due to the low cost of its simple camera sensor, which translates to low-weight equipment that allow the application of this method even from light unmanned aerial vehicles (UAV) [18,19].

However, the application of image velocimetry methods is not straightforward. According to Pearce et al. [20] "Some algorithms require additional effort for calibration and pre-processing. For example, with LSPIV and LSPTV, extensive training is required for an inexperienced user to define the appropriate parameters for an accurate surface flow velocity calculation." Indeed, Pearce et al. conducted sensitivity analyses on five image velocimetry algorithms (namely LSPIV, LSPTV, SSIV, KLT, and OTV). More specifically, they ran all algorithms with four extraction rates and three configurations, with each configuration having a different interrogation area (IA) size. They devised a sensitivity score based on the deviation between the configuration-specific velocity and the median cell velocity. This score demonstrated that the range of variation of the average velocity obtained by some of these algorithms was up to 75% of the average cross-sectional velocity ([20], Figure 7).

The selection of the most suitable IA size for each case study is not straightforward. Larger IA sizes allow, on the one hand, an improved signal-to-noise ratio; however, on the other hand, they result in lower cross-correlation peak values, which reduce the reliability of the detected velocity vectors [21]. For this reason, some image velocimetry algorithms employ multi-pass or ensemble correlation approaches, where the IA size is gradually reduced after each pass. The displacement information obtained from the initial passes is used to offset the IA in the following passes [22].

Besides the IA size, image velocimetry methods usually involve additional parameters. For example, Fudaa-LSPIV [23] needs to define the minimum and maximum acceptable correlation and PIVlab [22] needs to define the tile size of the contrast-limited adaptive histogram equalization (CLAHE) algorithm. These parameters, like the IA size, may have a significant impact on the accuracy

of the method, yet they are not directly related to any physical property (IA is influenced by the particle size and features density, but there is no mathematical formula to estimate the optimum size); rather their definition is based on intuition and requires expertise.

In this study, we suggest a statistical approach to address the above issues—the subjectivity of the selection of the parameter values and the impact of parameter uncertainty on the results of the image velocimetry method. For this reason, a probability distribution is defined for each model parameter. Then, Monte Carlo simulations can be employed to produce the confidence intervals of the estimated surface velocity, which give the estimated impact of parameter uncertainty on the results. Furthermore, the accuracy of the mean line of the confidence interval as an estimator of the velocity profile is investigated. This approach has two advantages: first, it involves the concept of the multi-pass approach, which, as mentioned previously, has been proven to be advantageous; and second, it reduces the impact of the subjectivity, which is limited to the definition of the probability distribution parameters. The impact of the latter subjectivity is evidently much lower than the impact of the subjectivity introduced when defining the image velocimetry algorithm parameters directly.

## 2. Materials and Methods

The image velocimetry tool employed in this study was Free-LSPIV [24] (see Supplementary Materials). In order to improve the sharpness of the video frames, Free-LSPIV employs application of the Gaussian blur filter, image subtraction, conversion to greyscale, and contrast adjustment; the latter involves turning off all the pixels with brightness lower than a threshold. To define this threshold, the contrast adjustment parameter is employed. The threshold is the product of this parameter by the maximum brightness value of the processed area. A parameter value equal to 1 means all pixels, except for the brightest, are turned off. A value equal to 0 means none of the pixels are turned off. Any value between 0.3 and 0.9 can be considered a plausible value (see Figure A1 in Appendix A).

Free-LSPIV uses fast normalized cross-correlation [25,26] between the IA (taken from a video frame) and the search area (taken from the next video frame). The location of the maximum value in the resulting correlation matrix gives the most probable displacement between the two frames. In some cases, the maximum value of this matrix may correspond to irrelevant particles. For example, in the case where IA contains only one particle just about to exit the IA with the flow, and the search area contains only one particle just entering. To filter out these cases, a parameter that defines the minimum acceptable cross-correlation is used. The location of the maximum value in the correlation matrix is considered valid displacement only if this value is greater than the minimum acceptable cross-correlation. From a mathematical perspective, this parameter value can be between  $-1$  and  $1$ , but for this application, it is more reasonable to select a value for the parameter between 0.3 (a value equal to 0 would not filter noise) and 0.9 (a value equal to 1 would mean the IA remains unchanged between successive frames).

Therefore, any Free-LSPIV application requires defining three parameters: the contrast adjustment, the minimum acceptable cross-correlation, and the IA size. The search area size can be obtained by appropriately augmenting the IA size to ensure the capacity to capture any possible particle displacement of the studied flow conditions.

The influence of the aforementioned parameters on the accuracy of Free-LSPIV was studied by employing Monte Carlo simulations. This included multiple runs of Free-LSPIV with different sets of parameter values. It should be noted that the methodology is not specific to Free-LSPIV and can be applied to any image velocimetry method that requires a definition of IA and other parameters. In fact, Monte Carlo simulations were employed for a similar purpose by Keane and Adrian [27,28].

The standard approach in Monte Carlo simulations is to generate random numbers using the triangular distribution [29,30] for obtaining the values of the parameters. Since the CPU time required for the execution of image velocimetry algorithms is considerable, it is not feasible to employ a large number of iterations. For this reason, and to ensure that the spread of the values produced by the

random number generator is as wide as possible (but always inside the prescribed limits), Equation (2) was used to produce the random numbers:

$$x_i = \Phi_{\text{TR}}(i/(n + 1); a, b, c), i = 1 \dots n \quad (2)$$

where  $x_i$  is the  $i$ th value from the total  $n$  values produced by the random number generator,  $\Phi_{\text{TR}}$  is the inverse cumulative of the triangular distribution function, and,  $a$ ,  $b$ , and  $c$  (with  $a < c < b$ ) are the parameters of the triangular distribution.

The distribution parameters  $a$ ,  $b$ , and  $c$  of the triangular distribution correspond to the plausible minimum, plausible maximum, and most likely values of the variable, respectively. The  $(a, b, c)$  values for the three studied parameters, i.e., the contrast adjustment parameter, the minimum acceptable cross-correlation, and the IA size were  $(0.3, 0.9, 0.7)$ ,  $(0.3, 0.9, 0.6)$ , and  $(\frac{1}{2}L, 2L, L)$ , respectively. In the last triplet,  $L$  is the mean IA side length in pixels (IAs are squares) of the  $n$  different IAs that were employed in the Monte Carlo simulations. Using Equation (2),  $n$  values were produced for each one of the three Free-LSPIV parameters. Then  $n^3$  sets of parameter values were formed employing the Cartesian product on the three sets of which each one has  $n$  generated parameter values. Free-LSPIV was run for each one of these  $n^3$  sets. This produced  $n^3$  velocity profiles along the cross-section from which the lower limit of the 90% confidence interval, the mean value, and the upper limit were derived.

The video and measurements used in this study were obtained from the data made publicly available by Pearce et al. [20]. Pearce et al. recorded two videos, Video A and Video B, of the flow of the Kolubara River near the city of Obrenovac in Central Serbia. The resolution of the videos is  $3696 \times 4994$ , their length is 25 and 21 s, respectively, and the frame rate is 23 fps. They also performed ADCP measurements along two cross-sections, named S1 and S2. The two videos combined with the two cross-sections resulted in four different datasets, which were used for testing the suggested methodology.

As mentioned previously, the CPU time of the image velocimetry methods is considerable. For this reason, it was initially investigated whether Equation (2) helps to obtain reliable estimations of the statistical profiles (lower limit, mean, and upper limit) with a limited number of iterations. For this reason, Monte Carlo simulations were applied to cross-section S1 of Video A with  $n = 20$  ( $20^3$  runs) and  $n = 5$  ( $5^3$  runs). The results of these simulations were compared to evaluate the sufficiency of a limited number of simulations to successfully capture the influence of uncertainty of parameters on the results.

Afterward, the information provided by the width of the zone between the lower and the upper limit of the 90% confidence interval was examined. It should be noted that this width represents only the uncertainty attributed to the parameters. The errors due to the intrinsic limitations of the image velocimetry methods were not captured. For example, in Pearce et al.'s study [20], all tested methods failed to correctly estimate the velocities near the right bank ([20], Figure 8) because surface features were sparse. This error cannot be avoided regardless of the selected parameter values.

It should be noted that  $L$  is the only parameter of the suggested method. It defines the IA sizes, which, for the given  $(a, b, c)$  values, range from  $L/2 \times L/2$  to  $2L \times 2L$ . A similar choice of multiple IA sizes is employed in PIVlab. According to Thielicke [31], PIVlab's accuracy is improved by employing three passes with IA sizes that are consecutive multiples of two. The optimum value of  $L$  depends on the density of the features captured by the video (more specifically the image density, i.e., the mean number of particle image pairs per interrogation volume [32]), the flow conditions, and the camera position. An empirical rule was derived in order to select the optimum  $L$  based on the confidence interval width. For this reason, the influence of  $L$  on the confidence interval width and the relation of the confidence interval width to the model accuracy were investigated. To do so, various  $L$  values were selected manually and then Monte Carlo simulations were executed (see Figure 1). After a series of Monte Carlo simulations with different  $L$  values, a group of results was compiled comprising the manually selected  $L$  value, the corresponding confidence interval width, and the accuracy of the mean profile compared to the ADCP velocity profile.

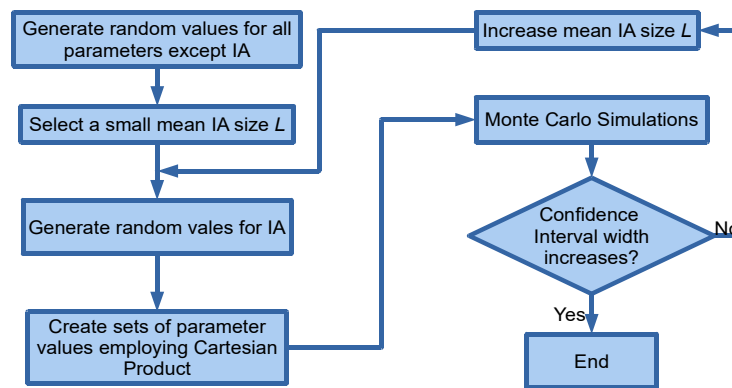


Figure 1. Schematic representation of Monte Carlo simulations to obtain the optimum mean IA size.

As mentioned previously, the multi-pass approach has been suggested to improve the accuracy of the particle image velocimetry methods. In this approach, information exchange takes place between successive passes by using the results of a preceding pass to offset the IA of the following pass [22]. This indicates that blending the information obtained with various IAs is advantageous. For this reason, the mean velocity profile produced by Monte Carlo simulations, which is an amalgamation of all simulation results, may be advantageous, in the same sense the multi-pass approach is advantageous over single runs.

### 3. Results

#### 3.1. Reliability of Monte Carlo Simulations with Low Number of Iterations

Monte Carlo simulations were executed with  $L$  values equal to 16, 32, and 64. These simulations were executed first with  $n = 5$  and then with  $n = 20$ . As mentioned previously, the sets of parameter values that were used in the Monte Carlo simulations were obtained by the Cartesian product:

$$\{x1_i\} \times \{x2_i\} \times \{x3_i\}, i = 1 \dots n \tag{3}$$

where  $x1_i$  are the values of the contrast adjustment obtained by Equation (2) for  $(a, b, c) = (0.3, 0.9, 0.7)$ ,  $x2_i$  are the values of the minimum acceptable cross-correlation obtained by Equation (2) for  $(a, b, c) = (0.3, 0.9, 0.6)$ , and  $x3_i$  are the values the IA size obtained by Equation (2) for  $(a, b, c) = (0.5 L, 2.0 L, 1.0 L)$ .

Figures 2–4 display the statistical profiles obtained by the Monte Carlo simulations with the three  $L$  and the two  $n$  values.

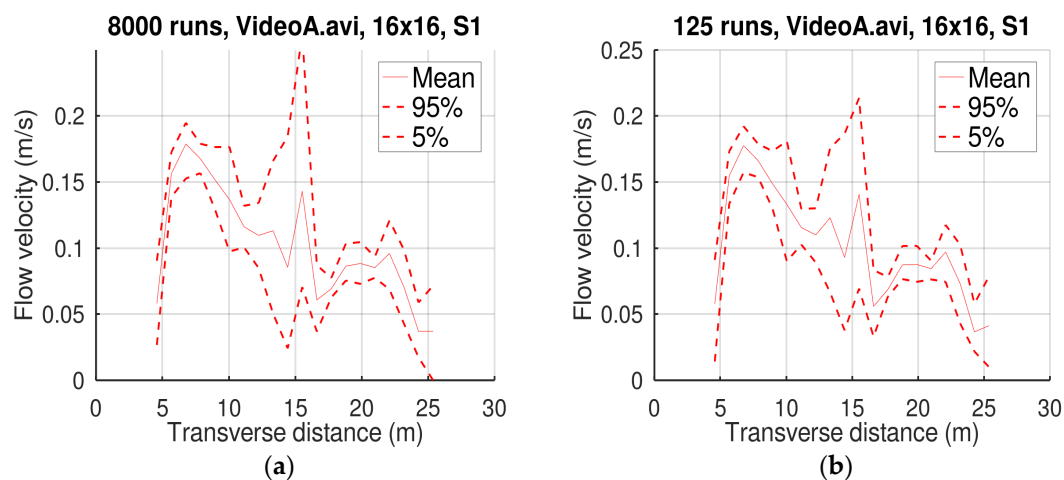
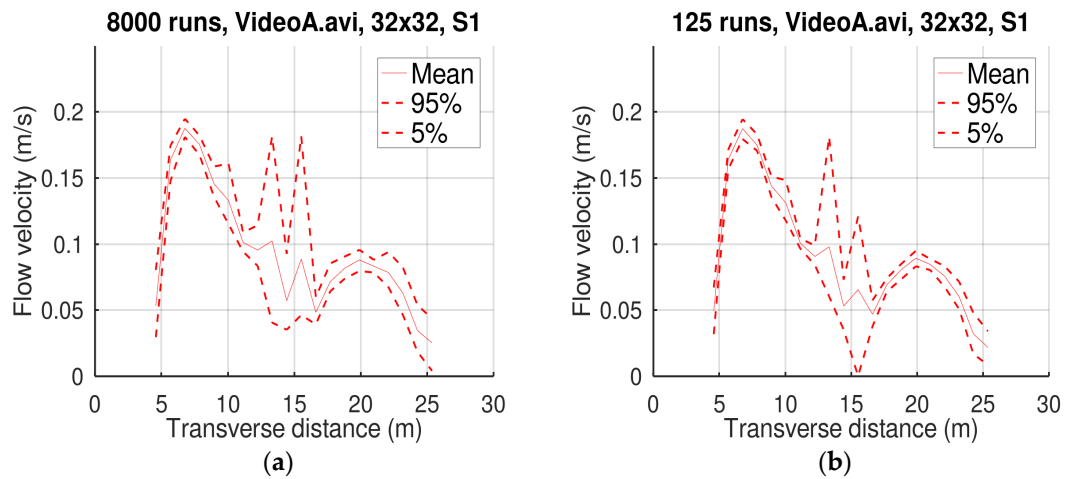
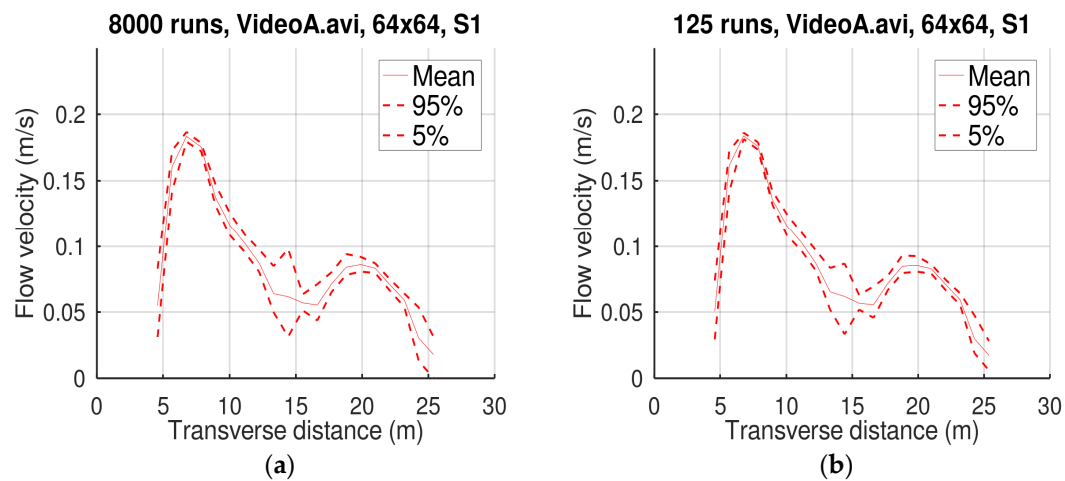


Figure 2. Mean velocity profile and confidence intervals of Monte Carlo simulations with  $20^3$  (a) and  $5^3$  (b) runs, and  $L = 16$ .



**Figure 3.** Mean velocity profile and confidence intervals of Monte Carlo simulations with  $20^3$  (a) and  $5^3$  (b) runs, and  $L = 32$ .



**Figure 4.** Mean velocity profile and confidence intervals of Monte Carlo simulations with  $20^3$  (a) and  $5^3$  (b) runs, and  $L = 64$ .

The CPU time required on a 3.5 GHz dual-core CPU laptop running MATLAB 2020a to perform the required Monte Carlo simulations is given in Table 1.

**Table 1.** CPU time required to perform Monte Carlo simulations.

$L$ (px)	$20^3$ Runs (Sec)	$5^3$ Runs (Sec)
64	88,718	1235
32	19,360	323
16	5208	86

The similarity between the mean, lower, and upper limits obtained with  $5^3$  and  $20^3$  runs was evaluated employing the Nash Sutcliffe Efficiency (NSE) coefficient. The results are shown in Table 2.

**Table 2.** NSE coefficient of the statistical profiles obtained with  $20^3$  and  $5^3$  runs.

$L$ (px)	Lower Limit	Mean	Upper Limit
64	0.99809	0.99977	0.99405
32	0.95002	0.98379	0.87227
16	0.97966	0.99298	0.95515

### 3.2. The Impact of the Mean IA Size on the Confidence Intervals

Figures 5 and 6 display the relation of the average width of the 90% confidence interval with the mean IA size ( $L \times L$ ). These figures correspond to the two videos and the two control cross-sections of Pearce et al. [20]. These figures also display the accuracy (NSE coefficient) of the mean velocity profile obtained by the Monte Carlo simulations using the corresponding ADCP measurements as reference values. The  $L$  values used in these Monte Carlo simulations were 128, 96, 64, 32, and 16. The value of  $n$  was 5 (125 runs).

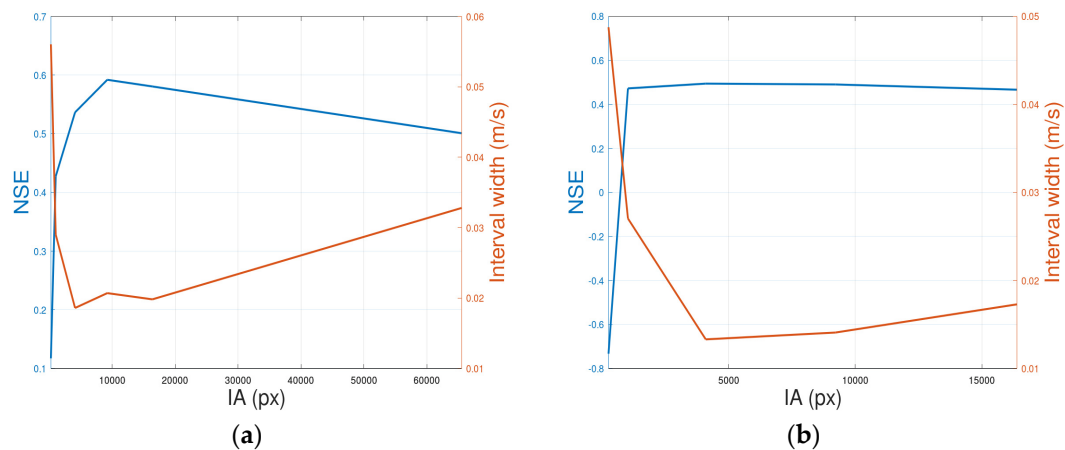


**Figure 5.** The impact of the mean IA size ( $L \times L$ ) on the accuracy of the estimated velocities and the 90% confidence interval width for Video A and the cross-sections S1 (a) and S2 (b).

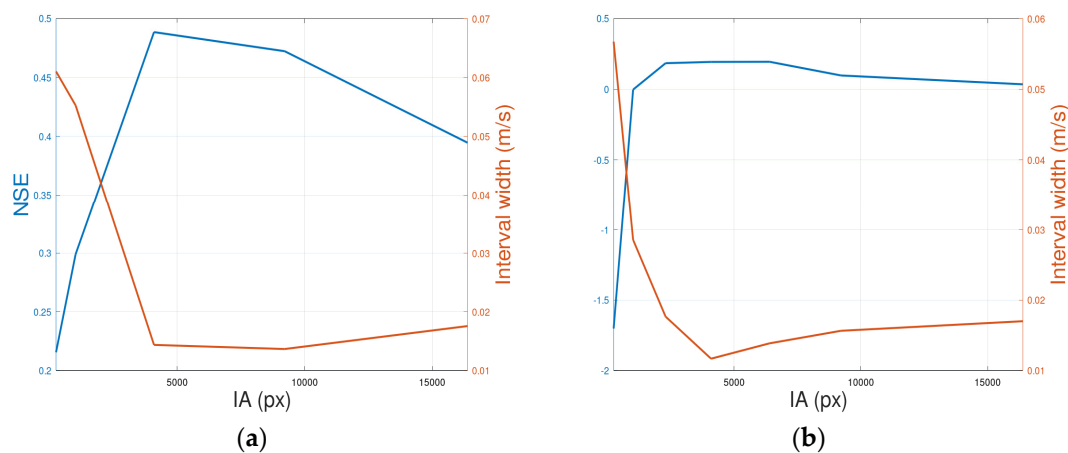


**Figure 6.** The impact of the mean IA size ( $L \times L$ ) on the accuracy of the estimated velocities and the 90% confidence interval width for Video B and the cross-sections S1 (a) and S2 (b).

### 3.3. Mean Velocity of Monte Carlo Simulations as Estimator of Cross-Section Velocity Profile

The following figures (Figures 7 and 8) display the result of the Monte Carlo simulations, the result of a single-run LSPIV applied by Pearce et al. [20], and the corresponding measurements obtained by the ADCP.

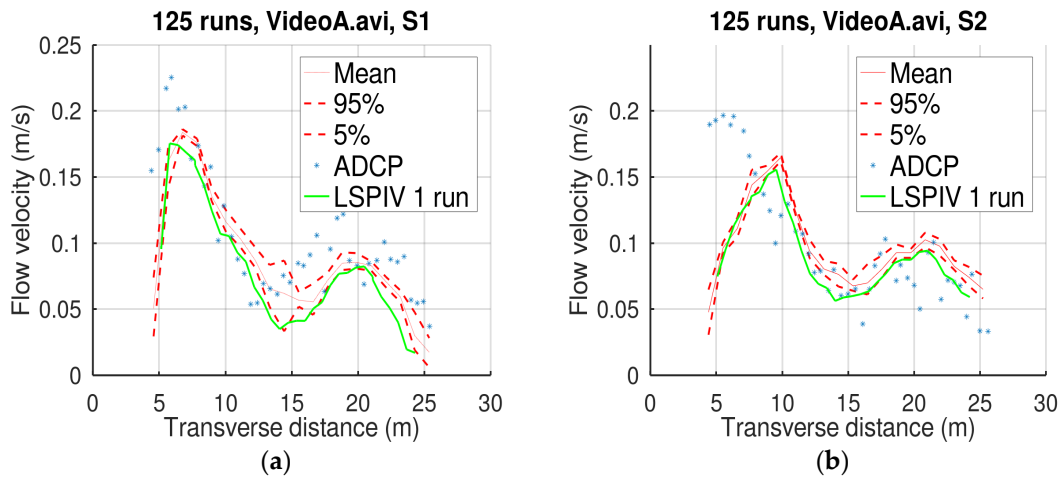


**Figure 7.** Velocity profiles and measurements for Video A and the cross-sections S1 (a) and S2 (b).

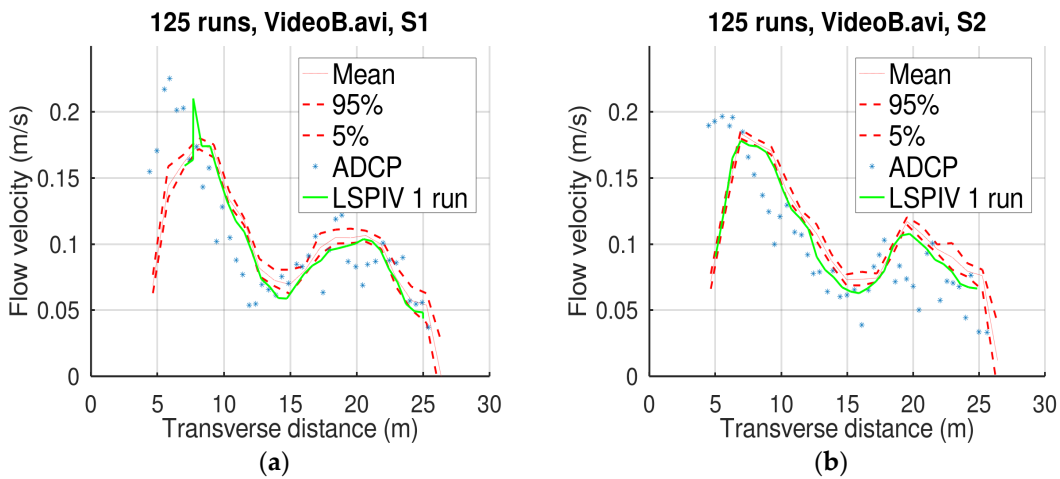


**Figure 8.** Velocity profiles and measurements for Video B and the cross-sections S1 (a) and S2 (b).

Table 3 gives the relative errors of the estimated discharge at the cross-sections S1 and S2 for videos A and B. The discharge was estimated using Equation (1) assuming a velocity coefficient equal to 0.85 to obtain  $v_i$  (the average velocity of the midsection of the  $i$ th segment) from the corresponding surface velocities [11]. The surface velocities of the single run LSPIV were obtained from Pearce et al. [20]. The reference discharge was estimated from the surface velocities of the ADCP measurements. The reason for doing so (instead of directly using the discharge estimated by the ADCP method) was to exclude the influence of the error of the estimation of  $v_i$  (from the surface velocity) from the comparisons.

**Table 3.** Relative error of the estimated discharge.

	Monte Carlo Mean	LSPIV Single Run
<b>Video A S1</b>	−10.34%	−22.27%
<b>Video A S2</b>	3.79%	−7.21%
<b>Video B S1</b>	3.79%	−1.71%
<b>Video B S2</b>	16.42%	9.56%

#### 4. Discussion

The comparisons of the Monte Carlo results with  $20^3$  and  $5^3$  runs displayed in Figures 2–4 and in Table 2 suggest that the use of Equation (2) for generating random numbers helped reliably estimate

the statistical profiles even with a limited number of simulations. This is very important taking into account the considerable CPU time required by image velocimetry methods.

Regarding the selection of the IA size, this remains a challenge despite techniques like the multi-pass approach or the Monte Carlo simulations used in this study. In both approaches, a mean IA size is defined and simulations with a range of IA sizes surrounding the mean value are performed. Figures 5 and 6 demonstrate the importance of the mean value. In all cases, the accuracy of the estimated velocities initially increased with the IA size, and then either stabilized or deteriorated. This is compatible with the findings of other researchers [21] who observed that larger IA sizes allow to improve the signal-to-noise ratio, but at the same time result in lower cross-correlation peak values, which reduces the confidence on the detected velocity vectors. Additionally, larger IA sizes reduce the effective resolution [33], which has a negative impact on the accuracy. Therefore, it is crucial to select the optimal IA size for each application. Figures 5 and 6 give an interesting hint. The IA size that achieved the best accuracy was close to the IA size that achieved the narrowest confidence interval. Therefore, with a series of Monte Carlo simulations with various mean IA sizes (Figure 1), one can obtain an indication of the optimum IA size.

The rest of the Free-LSPIV parameters do not vary greatly over different applications (always ranging between 0.3 and 0.9). These parameters do not require any handling. In single-run applications, one needs to subjectively select a value for these parameters. However, when Monte Carlo simulations are employed, there is no need for the selection of a specific value. The influence of uncertainty regarding the values of these parameters on the results is quantified by the confidence interval.

Figures 7 and 8 and Table 3 suggest that the mean profile of the Monte Carlo simulations achieved better accuracy than the LSPIV with a single run. The suggested methodology exhibited a relative bias of 13.66% in this specific application (Kolubara River). The LSPIV with a single run exhibited a relative bias of −21.63% for the specific PIVlab parameters selected by Pearce et al. for this application. If Monte Carlo simulations were used with PIVlab, PIVlab could have exhibited lower bias that may be lower than that of Free-LSPIV.

Finally, a long-term benefit of using Monte Carlo simulations is the full exploration of the peculiarities of the employed image velocimetry algorithm. For example, if the mean profile consistently overestimates or underestimates the surface velocities in many different applications, then this would be an indication that the algorithm introduces a systematic bias. This would allow to fine-tune the algorithm to remove this bias or introduce correction coefficients.

The following steps are suggested to improve the accuracy of an image velocimetry method with Monte Carlo simulations:

1. Identify the parameters of the method and their plausible maximum/minimum and most likely values.
2. Employ Equation (2) to generate sets of random values for the parameters. A small number of values (e.g.,  $n = 5$ ) for each parameter is sufficient.
3. Start with a low value for mean IA size (e.g.,  $L \times L = 16 \times 16$  pixels) and produce a small number (e.g.,  $n = 5$ ) of IA sizes employing Equation (2) with  $(a, b, c) = (\frac{1}{2}L, 2L, L)$ .
4. Run Monte Carlo simulations and obtain the mean and the lower and upper limits.
5. Increase  $L$  by a factor between 1 and 2. The confidence interval width will initially decrease with  $L$ . When the confidence interval stops decreasing with  $L$ , go to the next step, otherwise repeat steps 3 and 4.
6. Identify the Monte Carlo simulation with the lowest confidence interval width and use the mean velocity profile of this simulation as the best estimation of the surface velocities.

It should be noted that the confidence interval produced by the Monte Carlo simulations, as described above, does not consider the errors due to the intrinsic limitations of the image velocimetry methods. This type of error is currently under investigation. For example, Dal Sasso et al. [34] introduced a metric to evaluate the density and characteristics of the features on the surface of

flowing water, which helps obtain a prior estimation of the error of the image velocimetry method. Perks et al. [35] recently made available a range of datasets that were compiled from across six countries. These data could serve as the test bed for deriving a method that would estimate the overall error from both sources.

Finally, it should be noted that repeated Monte Carlo applications with different  $L$  values, instead of a single application of Monte Carlo with a very wide range of IA sizes, are recommended for various reasons. First, a very wide range would include large IA size values to Monte Carlo simulations, which, if far from the optimum  $L$  value, would result in an unnecessary increase of CPU time (see Table 1). Second, a low  $n$  value with a large parameter space would result in a poor representation of this space by the  $n$  generated random values. Finally, the confidence interval would be much wider than that of the previously described steps.

## 5. Conclusions

In this study, the uncertainty of the parameters of the particle image velocimetry method was investigated. The optimum values of these parameters depend on the flow conditions and on the camera position; however, there is no empirical rule to guide the selection of values for these parameters—it is rather based on the researchers' intuition. To avoid this subjectivity and estimate the influence of the uncertainty of the parameters on the results, Monte Carlo simulations were employed. The applications of this method demonstrated that the interrogation area size has a profound effect on the results and requires repeated applications of Monte Carlo simulations with different ranges. The other parameters do not require any handling. It was also found that the mean velocity profile obtained by Monte Carlo simulation tends to be more accurate than the result of a single run of a particle image velocimetry method. The uncertainty accounted for by this method does not include the errors caused due to the intrinsic limitations of image velocimetry methods, which have to do with the density and characteristics of the features on the surface of the flowing water. There is ongoing research on the error caused due to these limitations and methods. One could obtain the overall uncertainty of an image velocimetry method by combining these two sources of uncertainty.

**Supplementary Materials:** Free-LSPIV is available online at [www.hydroshare.org/resource/e713f959ad564adf8acacf1687250ea0/](http://www.hydroshare.org/resource/e713f959ad564adf8acacf1687250ea0/).

**Author Contributions:** Conceptualization, E.R., P.D., A.K.; methodology, E.R.; software, E.R.; validation, A.K. and K.M.; formal analysis, E.R.; resources, K.M.; data curation, S.L.; writing—original draft preparation, E.R.; writing—review and editing, A.K. and P.D.; visualization, E.R.; supervision, E.R. and A.K.; project administration, K.M.; funding acquisition, K.M. All authors have read and agreed to the published version of the manuscript.

**Funding:** The authors acknowledge the funding from the Hellenic General Secretariat for Research and Technology, under the National Strategic Reference Framework (2014–2020), for the project HYDRO-NET: Hydro-Telemetric Networks of Surface Waters: Gauging instruments, smart technologies, installation and operation, as a part of the Hellenic Integrated Marine and Inland Water Observing, Forecasting and Offshore Technology System, HIMIOFoTS (MIS5002739).

**Conflicts of Interest:** The authors declare no conflict of interest. The funders had no role in the design of the study; in the collection, analyses, or interpretation of data; in the writing of the manuscript, or in the decision to publish the results.

## Appendix A

The following figure displays the effects of the pre-processing of the video frames by Free-LSPIV [24].

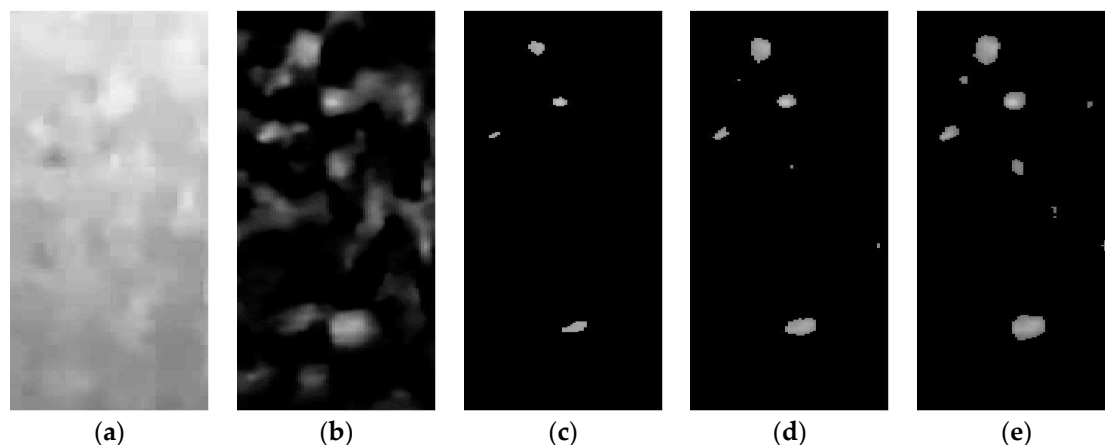


**Figure A1.** The effects of the Free-LSPIV pre-processing on a video frame: original greyscale (a), background removal (b), contrast adjustment with parameter 0.8 (c), contrast adjustment with parameter 0.7 (d), contrast adjustment with parameter 0.6 (e).

## References

1. Rozos, E. A methodology for simple and fast streamflow modelling. *Hydrol. Sci. J.* **2020**, *65*, 1084–1095. [[CrossRef](#)]
2. Rozos, E. Machine learning, urban water resources management and operating policy. *Resources* **2019**, *8*, 173. [[CrossRef](#)]
3. World Meteorological Organization. *Manual on Stream Gauging Vol. 1 Fieldwork*; WMO-No.1044; World Meteorological Organization: Geneva, Switzerland, 2010.
4. Hauet, A. Stream gauging techniques. In *Course on Stream Gauging*; IAHR WMO IAHS Training: Lyon, France, 2018.
5. Kasvi, E.; Laamanen, L.; Lotsari, E.; Alho, P. Flow patterns and morphological changes in a sandy meander bend during a flood—Spatially and temporally intensive ADCP measurement approach. *Water* **2017**, *9*, 106. [[CrossRef](#)]
6. Adrian, R.J. Particle-imaging techniques for experimental fluid mechanics. *Annu. Rev. Fluid Mech.* **1991**, *23*, 261–304. [[CrossRef](#)]
7. Fujita, I.; Muste, M.; Kruger, A. Large-scale particle image velocimetry for flow analysis in hydraulic engineering applications. *J. Hydraul. Res.* **1998**, *36*, 397–414. [[CrossRef](#)]
8. Muste, M.; Fujita, I.; Hauet, A. Large-scale particle image velocimetry for measurements in riverine environments. *Water Resour. Res.* **2008**, *44*, 1–14. [[CrossRef](#)]
9. Le Boursicaud, R.; Pénard, L.; Hauet, A.; Thollet, F.; Le Coz, J. Gauging extreme floods on YouTube: Application of LSPIV to home movies for the post-event determination of stream discharges. *Hydrol. Process.* **2016**, *30*, 90–105. [[CrossRef](#)]
10. Al-Mamari, M.M.; Kantoush, S.A.; Kobayashi, S.; Sumi, T.; Saber, M. Real-time measurement of flash-flood in a Wadi Area by LSPIV and STIV. *Hydrology* **2019**, *6*, 27. [[CrossRef](#)]
11. Rantz, S.E. Measurement and computation of streamflow. In *Measurement and Computation of Streamflow*; US Geological Survey: Reston, VA, USA, 1982; Volume 1, p. 137.
12. Chiu, C.L. Entropy and 2-D velocity in open channels. *J. Hydraul. Eng.* **1988**, *114*, 738–756. [[CrossRef](#)]
13. Dimitriadis, P.; Koussis, A.; Koutsyiannis, D. Estimating the hydraulic profiles in a cross-section under one-dimensional steady-flow dynamics by employing the entropy maximization principle: I. Theoretical concepts. *RG* **2019**. [[CrossRef](#)]
14. Dimitriadis, P.; Rozos, E.; Mazi, K.; Koussis, A. Estimating the hydraulic profiles in a cross-section under one-dimensional steady-flow dynamics by employing the entropy maximization principle: II. Applications. *RG* **2019**. [[CrossRef](#)]
15. Bechle, A.J.; Wu, C.H.; Liu, W.-C.; Kimura, N. Development and application of an automated river-estuary discharge imaging system. *J. Hydraul. Eng.* **2012**, *138*, 327–339. [[CrossRef](#)]

16. Bradley, A.; Kruger, A.; Meselhe, E.; Muste, M. Flow measurement in streams using video imagery. *Water Resour. Res.* **2002**, *38*. [[CrossRef](#)]
17. Tauro, F.; Piscopia, R.; Grimaldi, S. Streamflow observations from cameras: Large-scale particle image velocimetry or particle tracking velocimetry? *Water Resour. Res.* **2017**, *53*, 10374–10394. [[CrossRef](#)]
18. LeGrand, M.; Luce, J.; Metcalfe, R.; Buttle, J. Development of an inexpensive automated streamflow monitoring system. *Hydrol. Process.* **2020**, *34*, 3021–3023. [[CrossRef](#)]
19. Manfreda, S.; McCabe, M. Emerging earth observing platforms offer new insights into hydrological processes. *HydroLink* **2019**, *1*, 8–9.
20. Pearce, S.; Ljubičić, R.; Peña-Haro, S.; Perks, M.T.; Tauro, F.; Pizarro, A.; Sasso, S.F.D.; Strelnikova, D.; Grimaldi, S.; Maddock, I.; et al. An evaluation of image velocimetry techniques under low flow conditions and high seeding densities using unmanned aerial systems. *Remote. Sens.* **2020**, *12*, 232. [[CrossRef](#)]
21. Raffel, M.; Willert, C.; Scarano, F.; Kähler, C.J.; Wereley, S.T.; Kompenhans, J. *Particle Image Velocimetry: A Practical Guide*, 3rd ed.; Springer International Publishing AG: Cham, Switzerland, 2018.
22. Thielicke, W.; Stamhuis, E. PIVlab—Towards user-friendly, affordable and accurate digital particle image velocimetry in MATLAB. *J. Open Res. Softw.* **2014**, *2*, 1202. [[CrossRef](#)]
23. Le Coz, J.; Jodeau, M.; Hauet, A.; Marchand, B.; Le Boursicaud, R. Image-based velocity and discharge measurements in field and laboratory river engineering studies using the free Fudaa-LSPIV software. In Proceedings of the International Conference on Fluvial Hydraulics, RIVER FLOW 2014, Lausanne, Switzerland, 3–5 September 2014; pp. 1961–1967.
24. Rozos, E.; Dimitriadis, P.; Mazi, K.; Lykoudis, S.; Koussis, A. Application of a Simple Image Velocimetry Algorithm in hydrometry. *RG* **2020**. [[CrossRef](#)]
25. Keane, R.D.; Adrian, R.J. Theory of cross-correlation analysis of PIV images. *Appl. Sci. Res.* **1992**, *49*, 191–215. [[CrossRef](#)]
26. Lewis, J.P. Fast Template matching. *Vis. Interface* **1995**, *95*, 120–123.
27. Keane, R.; Adrian, R. Optimization of particle image velocimeters. I. Double pulsed systems. *Meas. Sci. Technol.* **1990**, *1*, 1202–1215. [[CrossRef](#)]
28. Keane, R.D.; Adrian, R.J. Optimization of particle image velocimeters: II. Multiple pulsed systems. *Meas. Sci. Technol.* **1991**, *2*, 963–974. [[CrossRef](#)]
29. Sprow, F.B. Evaluation of research expenditures using triangular distribution functions and monte carlo methods. *Ind. Eng. Chem.* **1967**, *59*, 35–38. [[CrossRef](#)]
30. Saha, G.C.; Li, J.; Thring, R.W. Understanding the effects of parameter uncertainty on temporal dynamics of groundwater-surface water interaction. *Hydrology* **2017**, *4*, 28. [[CrossRef](#)]
31. Thielicke, W. PIVlab Tutorial. Available online: [https://pivlab.blogspot.com/p/blog-page\\_19.html](https://pivlab.blogspot.com/p/blog-page_19.html) (accessed on 28 July 2020).
32. Kähler, C.J.; Scharnowski, S.; Cierpka, C. On the resolution limit of digital particle image velocimetry. *Exp. Fluids* **2012**, *52*, 1629–1639. [[CrossRef](#)]
33. Adrian, R. Twenty years of particle image velocimetry. *Exp. Fluids* **2005**, *39*, 159–169. [[CrossRef](#)]
34. Sasso, S.F.D.; Pizarro, A.; Manfreda, S. Metrics for the quantification of seeding characteristics to enhance image velocimetry performance in rivers. *Remote Sens.* **2020**, *12*, 1789. [[CrossRef](#)]
35. Perks, M.T.; Sasso, S.F.D.; Hauet, A.; Jamieson, E.; Le Coz, J.; Pearce, S.; Peña-Haro, S.; Pizarro, A.; Strelnikova, D.; Tauro, F.; et al. Towards harmonisation of image velocimetry techniques for river surface velocity observations. *Earth Syst. Sci. Data* **2020**, *12*, 1545–1559. [[CrossRef](#)]

